or alcohols and is weakly solvated (~-2 to -5 kJ mol^{-1}), compared with its state in water, in the region x_{ROH} from 0.1 to 0.4. At higher mole fractions the cation is destabilized; however, high-pressure kinetics measurements are not practicable in these mixtures. The results of Table IV show that the transition states in each aqueous alcohol mixture are slightly stabilized compared with those in water. Therefore, ΔV^* should reflect a decrease in desolvation relative to reaction in water for the $Fe^{II}(gmi)_3$ cation in aqueous alcohols. The results in Table III are qualitatively in agreement with this comparison of solvation probes. It is doubtful whether the partial contribution of each to ΔV^*_{solv} can be assessed quantitatively without detailed models and theoretical description.

The ΔV^* trends for the two small iron(II) cations, $Fe(gmi)_3^{2+}$ and $Fe(hxsb)^{2+}$ (for example, in 60% i-C_3H_7OH and 50% t-C_4H_9OH, ΔV^* is 4 and 8 cm^3 mol^{-1} less for $Fe(hxsb)^{2+}$), are different. The exterior of $Fe(hxsb)^{2+}$ is not particularly hydrophobic except for the quadrant containing two pyridine rings. By contrast a model of the structure of $Fe(gmi)_3^{2+}$ reveals two close groupings of each of three methyl moieties; thus, the fraction of total surface area that is hydrophobic, while still small, is higher in $Fe(gmi)_3^{2+}$ than in $Fe(hxsb)^{2+}$. This difference, and cation size difference, and the fact that $Fe(hxsb)^{2+}$ has potential hydrogen-bonding sites, could well be the sources of variation in ΔV^*. It could also be speculated that the decline of ΔV^* to a fairly similar value in each alcohol mixture is a reflection of an earlier transition state in which less desolvation occurs and is consistent with the increase in rate constant.

In contrast, the very large and hydrophobic $Fe((CH_3)_2bsb)_3^{2+}$ cation is progressively strongly solvated by methanol with increase in x_{CH_3OH}, as reported earlier.[20] For reaction with hydroxide ΔV^* increases to ~+25 cm^3 mol^{-1} (0-80% CH_3OH), implying a big contribution from methanol desolvation in the transition state; it is not clear why this occurs, unless the solvation of the complex is perturbed in the region of penetration by the charged hydroxide ion, since an overall charge reduction would not favor such desolvation. Size of the alcohol, as well as its intrinsic character may be a factor, since when the higher alcohols are used, while ΔV^* is increased over that for reaction of hydroxide with $Fe((CH_3)_2bsb)_3^{2+}$, the increase is much less pronounced, typically half as much as the same parameter in aqueous methanol. Results from other complexes being studied may lead to development of a clearer interpretation of results.

Acknowledgment. We thank the Royal Society and the SERC for grants toward the purchase and the construction of the Unicam SP 8-100 instrument and the high-pressure apparatus, respectively. The National Science Foundation grant (CHE-7908399) used for purchase of the Cary 219 spectrophotometer is gratefully acknowledged. C.D.H. thanks the Faculty Development Committee of the University of New Hampshire for a travel grant, and support from the British Council (P.G.) is greatly appreciated.

Supplementary Material Available: Listings of bond angles, bond lengths, fractional atomic coordinates, atomic thermal parameters, and nonbonded contacts (5 pages); tables of structure factors (7 pages). Ordering information is given on any current masthead page.

Contribution from the Departments of Chemistry, Iowa State University, Ames, Iowa 50011, and Texas A&M University, College Station, Texas 77843

Chains of Centered Metal Clusters with a Novel Range of Distortions: Pr_3I_3Ru, Y_3I_3Ru, and Y_3I_3Ir

Martin W. Payne, Peter K. Dorhout, Sung-Jin Kim, Timothy R. Hughbanks,* and John D. Corbett*

Received August 26, 1991

The phases R_3I_3Ru (R = La, Pr, Gd, Y, Er) and R_3I_3Ir (R = Gd, Y) are obtained from the reactions of R, RI_3, and Ru or Ir for 3-4 weeks in sealed Ta tubing at 850-975 °C, depending on the system. The title phases have been characterized by single-crystal X-ray means at room temperature, with space group $P2_1/m$ and $Z = 2$ (Pr_3I_3Ru, Y_3I_3Ru, Y_3I_3Ir, respectively: a = 9.194 (1), 8.7001 (4), 8.6929 (7) Å; b = 4.2814 (5), 4.1845 (2), 4.2388 (4) Å; c = 12.282 (2), 12.1326 (6), 12.092 (2) Å; β = 93.46 (1), 94.769 (5), 94.73 (1)°; R/R_w = 3.7/3.4, 3.2/5.5, 4.4/4.0%). The first phase contains quasi-infinite double chains of edge-sharing $Pr_6(Ru)$ octahedra that are sheathed and interbridged by iodine. An evidently continuous distortion of these chains parallels the a/b axial ratio (in the order listed in the first sentence) such that metal octahedra are no longer obvious in Y_3I_3Ir; rather chains of trans-edge-sharing square pyramidal Y_4Ir units bonded base-to-base are more apt. Increased R-R, R-interstitial, and interstitial-interstitial bonding appears to parallel the degree of distortion. Magnetic data for La_3I_3Ru and Pr_3I_3Ru and the results of extended Hückel band calculations on Pr_3I_3Ru are reported. Polar covalent Pr-Ru interactions and at least a quasi-closed shell configuration are emphasized by the latter.

Introduction

A most unusual and prolific chemistry is obtained when rare-earth-metal (R) halides—iodides especially—are reduced in the presence of many of the later transition metals. The dominant structural elements in the products are R_6I_{12}-type octahedral clusters that are either interconnected by iodide in $R(R_6I_{12})$[1] or R_6I_{10}[2,3] stoichiometries or condensed through shared trans metal edges into quasi-infinite chains of clusters. A most remarkable feature is that each cluster is centered by a transition-metal atom. The condensed structures are typified by the La_4I_5Ru and Pr_4I_5Z (Z = Co, Ru, Os) groups recently reported. These are predicted to be metallic according to band calculations.[4] Phases in which such chains are further condensed side-by-side to yield double chains have been long known in other systems, such as Sc_7Cl_{10}[5] and $Sc_7Cl_{10}C_2$[6] (=$Sc_6Cl_7C_2$·$ScCl_3$) and, more recently, $Y_6I_7C_2$,[7] $Gd_6I_7C_2$,[8] etc. The present article reports the first details regarding a different variety of double-chain phases that are now centered by 4d or 5d transition metals. The La_3I_3Ru and Pr_3I_3Ru examples are most analogous to the earlier structures just noted, while, in the distorted relatives Y_3I_3Ru, Y_3I_3Ir, and others, metal octahedra sharing trans and side edges can no longer be easily recognized.

Experimental Section

The purities of the starting metals, the sources of high-quality RI_3 reactants, the synthetic techniques utilizing sealed niobium containers, and the Guinier powder pattern methodology were as described earlier.[1-4]

Syntheses. The specific conditions leading to the black R_3I_3Z phases reported herein in high yield in 3-4 weeks are as follows. La, Ru:

(1) Hughbanks, T.; Corbett, J. D. *Inorg. Chem.* **1988**, *27*, 2022.
(2) Hughbanks, T.; Corbett, J. D. *Inorg. Chem.* **1989**, *28*, 631.
(3) Payne, M. W.; Corbett, J. D. *Inorg. Chem.* **1990**, *29*, 2246.
(4) Payne, M. W.; Dorhout, P. K.; Corbett, J. D. *Inorg. Chem.* **1991**, *30*, 1467, 3112.
(5) Poeppelmeier, K. R.; Corbett, J. D. *Inorg. Chem.* **1977**, *16*, 1107.
(6) Hwu, S.-J.; Corbett, J. D.; Poeppelmeier, K.R. *J. Solid State Chem.* **1985**, *57*, 43.
(7) Kauzlarich, S. M.; Hughbanks, T.; Corbett, J. D.; Klavins, P.; Shelton, R. N. *Inorg. Chem.* **1988**, *27*, 1791.
(8) Simon, A. *J. Solid State Chem.* **1985**, *57*, 2.

0020-1669/92/1331-1389$03.00/0

Table I. Cell Parameters (Å; deg) for Monoclinic R_3I_3Z Phases (Space Group $P2_1/m$)[a]

compd	lines	*a*	*b*	*c*	β	*a*/*b*
La_3I_3Ru	23	9.358 (1)	4.3510 (6)	12.487 (2)	93.62 (2)	2.151
Pr_3I_3Ru[b]	49	9.194 (1)	4.2814 (5)	12.282 (2)	93.46 (1)	2.147
Gd_3I_3Ru[c]	29	8.848 (8)	4.228 (3)	12.04 (1)	92.8 (1)	2.093
Y_3I_3Ru	93	8.7001 (4)	4.1845 (2)	12.1326 (6)	94.769 (5)	2.079
Er_3I_3Ru	33	8.6265 (6)	4.1590 (4)	12.063 (1)	95.071 (8)	2.074
Gd_3I_3Ir	41	8.7631 (7)	4.2496 (4)	12.190 (1)	94.75 (1)	2.062
Y_3I_3Ir[b]	50	8.6929 (7)	4.2388 (4)	12.092 (2)	94.73 (1)	2.051

[a] Guinier powder diffraction with Si as internal standard; λ = 1.540 56 Å. [b] Data crystal from the same sample. [c] The generally larger standard deviations found for Gd_3I_3Ru may imply distortion to a lower (triclinic) symmetry.

Table II. Selected Crystal and Refinement Data[a]

	Pr_3I_3Ru	Y_3I_3Ru	Y_3I_3Ir
space group, *Z*	$P2_1/m$ (No. 11), 2	$P2_1/m$ (No. 11), 2	$P2_1/m$ (No. 11), 2
V, Å^3	481.33 (9)	441.7 (4)	442.6 (3)
no. of unique reflns, $F_o^2 > 3\sigma(F_o^2)$	1366	688	1052
no. of params refined	44	43	44
μ(Mo Kα), cm^{-1}	258.5	315.8	464.2
transm factor range	0.82–1.28	0.536–1.00	0.870–1.19
R,[b] %	3.7	3.4	3.2
R_w,[c] %	5.5	4.4	4.0

[a] Lattice dimensional data in Table I. [b] $R = \sum||F_o| - |F_c||/\sum|F_o|$. [c] $R_w = [\sum w(|F_o| - |F_c|)^2/\sum w(F_o)^2]^{1/2}$; $w = [\sigma(F)]^{-2}$.

850–975 °C, stoichiometric conditions. Pr, Ru: 900–975 °C over a wide composition range with an excess of I and/or Ru relative to the correct stoichiometry; a Ru deficiency (4:5:1) gives the side product $Pr_7I_{12}Ru$ at 900 °C or Pr_4I_5Ru at 975 °C. Gd, Ru: 900–975 °C over a wide composition range. Gd, Ir: 850 °C for 2 weeks with 4:5:1 composition; 900 °C gives only $Gd_6I_{10}Ir$. Y, Ru: ~975 °C, stoichiometric conditions or with an excess or deficiency of Ru or a small excess of I; shorter times at lower temperatures yield $Y_{16}I_{20}Ru_4$.[9] Y, Ir: conditions similar to those for Z = Ru but giving $Y_6I_{10}Ir$ instead at 850 °C. Er, Ru: stoichiometric conditions or an iodine deficiency at 900–980 °C, with a new phase sometimes intruding.[10]

Guinier-based lattice constants for the new monoclinic R_3I_3Z phases are listed in Table I. Compounds with this structure were earlier[4] referred to as $R_6I_6Z_2$ types in order to distinguish them from the cubic R_3I_3Z examples (Gd_3Cl_3C type[11]) also known with some heavy transition metals.[12] However, this notation has been dropped, as it is crystallographically inconsistent.

Structural Studies. Needle crystals of the prototype phase Pr_3I_3Ru were obtained in high yield before the competing Pr_4I_5Ru had been characterized. Four octants of diffraction data were collected to 2θ = 60° at room temperature from a well-diffracting prismatic crystal of the former for the indicated primitive monoclinic cell. Five ψ scans taken as a function of 2θ and averaged were the basis of the initial absorption correction. Space group $P2_1/m$ was implied by the absences and averaging, and direct methods (SHELXS[13]) gave an immediate solution therein. Differences in anisotropic displacement parameters after a satisfactory refinement of the structure isotropically suggested an inadequate absorption correction had been applied (μ = 258 cm^{-1}), and DIFABS[14] again solved the problem. The Ru position refined to 99.4 (3)% occupancy and was thereafter returned to unity. The final difference Fourier map showed peaks of ≤4.8 e/Å^3, the largest being 1.1 Å from Pr1, while the disposition of extra peaks up to 13 e/Å^3 present in the Fourier map suggested termination effects. Selected data collection and refinement information is given in Table II, while more details are contained in the supplementary material.

The crystal structure of Y_3I_3Ir was investigated after its powder pattern and the lattice dimensions deduced therefrom suggested that the structure was appreciably different from that of Pr_3I_3Ru. A monoclinic cell was deduced by the diffractometer and its programs,[15] and data in four octants were collected from a well-diffracting prismatic crystal at room temperature out to 2θ = 60°. The Laue check confirmed the presence of a 2-fold axis parallel to *b*. The critical 0*k*0 reflections were scanned for odd *k* to ±7, and only very small shoulders on the sides of large peaks were encountered, so $P2_1/m$ again seemed probable. Absorption was ultimately corrected with the aid of four ψ scans in the range 19° ≤ 2θ ≤ 39°. The similarity of the lattice dimensions and symmetry to those of Pr_3I_3Ru suggested that the two structures were alike, yet refinement starting with the latter as a trial model produced an *R* of ~50%. Direct methods gave a closely related solution that was refined without event (Table II). Ir refined to 101.1 (3)% occupancy and was therefore returned to unity. The largest residue in the Δ*F* map was a peak of 2.4 e/Å^3 that was 0.8 Å from Ir. The structure is significantly distorted from that of Pr_3I_3Ru.

A crystal later determined to be the isostructural Y_3I_3Ru was encountered in an attempt to synthesize $Y_6I_{10}Ru$ for other purposes. The reaction was carried out at 950 °C for 21 days, as reported previously.[2] We presume that a somewhat YI_3-poor reaction mixture allowed the formation of Y_3I_3Ru along with $Y_6I_{10}Ru$. The structure was solved and refined independently and uneventfully from a direct-methods model.[15]

Magnetic Susceptibilities. Magnetic susceptibility measurements were carried out on several independently prepared samples of Pr_3I_3Ru and La_3I_3Ru on a Quantum Design-MPMS SQUID magnetometer at fields ranging from 0.01 to 2 T over a temperature range of 6–300 K with measurements every 10 K. More extensive low-temperature measurements at 0.01, 0.10, and 1.0 T were also made on the latter at 6–70 K with measurements every 2 K. Quantitative samples (30–50 mg) were held between two silica rods (3-mm o.d.) sealed inside 3-mm-i.d. silica tubes under ~1 atm of He, a design which gives much better behaved background signals. All reported data have been corrected for core diamagnetism with -2.4×10^{-4} emu mol^{-1}.

Band Calculations. One-dimensional extended Hückel band structure calculations were carried out at 16K points for the chain $^1_\infty[Pr_6I_6Ru_2(I^-)_4^{4-}]$ in which terminal iodine atoms had been added at all exo positions to simulate the bridge bonding, as in the case of Pr_4I_5Ru.[4] The crystallographic positions were used, while atom parameters were those derived for the Pr_4I_5Ru example. Since the structure contains chains of edge-sharing octahedra along a 2-fold screw axis, only the inversion center at Γ could be used to assign band symmetries. A smoothing parameter of 0.005 eV was applied to the DOS and COOP plots.

Results and Discussion

The synthesis of each of the new R_3I_3Z phases involves consideration not only of the particular interstitials (Z) but also of other stable structures and compositions that may incorporate the same elements. Some of the problems this can introduce have been noted in recent reports on the Y–I–Ru[9] and Pr–I–Ru[4] systems. Complex reactions and equilibria involving several alternatives can mean that the appearance or absence of a certain phase may be quite temperature as well as time dependent. In such cases, comparative interpretations and stability inferences are difficult and uncertain. For the monoclinic R_3I_3Z compounds reported here, the competitive cluster phases for each combination of the three elements are as follows: La_3I_3Ru–$La_7I_{12}Ru$ (new), La_4I_5Ru; Pr_3I_3Ru–$Pr_7I_{12}Ru$, Pr_4I_5Ru; Gd_3I_3Ru–$Gd_7I_{12}Ru$; Gd_3I_3Ir–$Gd_6I_{10}Ir$ (new), $Gd_7I_{12}Ir$; Y_3I_3Ru–$Y_{16}I_{20}Ru_4$,[9] $Y_7I_{12}Ru$, $Y_6I_{10}Ru$; Y_3I_3Ir–$Y_6I_{10}Ir$; Er_3I_3Ru–unknown phase; Er_3I_3Ir–unknown phases.[10] In addition, the following interstitial elements

(9) Payne, M. W.; Ebihara, M.; Corbett, J. D. *Angew. Chem., Int. Ed. Engl.* **1991**, *30*, 856.
(10) Ebihara, M.; Corbett, J. D. Unpublished research.
(11) Warkentin, E.; Simon, A. *Rev. Chim. Miner.* **1983**, *20*, 488.
(12) Dorhout, P. K.; Payne, M. W.; Corbett, J. D. *Inorg. Chem.* **1991**, *30*, 4960.
(13) Sheldrick, G. M. SHELXS-86. Institut für Anorganische Chemie, Universität Göttingen, FRG.
(14) Walker, N.; Stuart, D. *Acta Crystallogr.* **1983**, *A39*, 158.
(15) (a) *TEXSAN-TEXRAY Structure Analysis Package*; Molecular Structure Corp.: Woodlands, TX, 1985. (b) Gilmore, C. J. *J. Appl. Crystallogr.* **1984**, *17*, 42. (c) Beurskens, P. T. DIRDIF: Direct Methods for Difference Structures. Technical Report 1984/1; Crystallography Laboratory: Toernooiveld, 6525 Ed Nijmegen, The Netherlands, 1984.

Table III. Positional Parameters for the Monoclinic R_3I_3Z Structures

atom	x	y	z	B, Å^2
		Pr_3I_3Ru		
Pr1	0.09926 (5)	$^1/_4$	0.89156 (4)	0.565 (8)
Pr2	0.11857 (5)	$^1/_4$	0.33471 (4)	0.621 (8)
Pr3	0.31545 (5)	$^3/_4$	0.12092 (4)	0.593 (8)
I1	0.39450 (6)	$^3/_4$	0.86205 (5)	0.870 (9)
I2	0.37467 (6)	$^3/_4$	0.38238 (5)	1.03 (1)
I3	0.13865 (7)	$^1/_4$	0.61785 (5)	0.95 (1)
Ru	0.11112 (7)	$^1/_4$	0.12511 (5)	0.48 (1)
		Y_3I_3Ru		
Y1	0.1370 (2)	$^1/_4$	0.8700 (2)	1.27 (8)
Y2	0.1035 (2)	$^1/_4$	0.3218 (2)	1.35 (8)
Y3	0.2614 (2)	$^3/_4$	0.1078 (2)	1.35 (8)
I1	0.4291 (1)	$^3/_4$	0.8638 (1)	1.66 (6)
I2	0.3622 (1)	$^3/_4$	0.3716 (1)	1.57 (5)
I3	0.1459 (1)	$^1/_4$	0.6052 (1)	1.62 (5)
Ru	0.0519 (2)	$^1/_4$	0.0933 (1)	1.16 (6)
		Y_3I_3Ir		
Y1	0.1449 (2)	$^1/_4$	0.8684 (1)	0.64 (5)
Y2	0.1003 (2)	$^1/_4$	0.3203 (1)	0.81 (5)
Y3	0.2543 (2)	$^3/_4$	0.1020 (1)	0.73 (5)
I1	0.4322 (1)	$^3/_4$	0.86384 (8)	1.13 (4)
I2	0.3582 (1)	$^3/_4$	0.36873 (8)	1.10 (4)
I3	0.1459 (1)	$^1/_4$	0.60448 (7)	1.05 (3)
Ir	0.04785 (6)	$^1/_4$	0.09249 (4)	0.51 (2)

do not provide the monoclinic R_3I_3Z phase in each case: lanthanum—Re, Os, Rh, Ir, Pt; praseodymium—Fe, Cu, Ag, Re, Ir, Rh, Pt;[4] gadolinium—Mo, Re, Os; yttrium—Fe, Co, Re, Os, Rh, Pd, Pt; erbium—Re, Os, Pt.

Three structures have been quantified: the prototypes Pr_3I_3Ru and Y_3I_3Ru, which reflect the effects of a marked distortion with the same Z, and Y_3I_3Ir, which shows a still greater distortion with the same host metal and a slightly larger interstitial. The degree of distortion appears to scale roughly with the lattice dimension ratios a/b (Table I), which put the first and third named compounds near the extremes among the seven examples known in this structural regime. Positional parameters and important distances and angles for the three are listed in Tables III and IV, respectively. The structure of Pr_3I_3Ru will be considered first, since it is the most similar to other structures that contain comparable double chains of condensed metal octahedra that are each centered by a single interstitial atom.

Pr_3I_3Ru. The off-axis view of a section along the metal chains in Figure 1 shows the atom positions, their numbering and connectivities, and the primitive monoclinic cell. All atoms lie on mirror planes at $y = {}^1/_4$ or $^3/_4$, the latter being distinguished in the figure by dots. (An infinite projection of Gd_3I_3C published without any further details[16] has been confirmed to represent the same structure.[17]) The principal structural element is chains of $Pr_6I_{12}Ru$-type clusters that have been condensed through sharing of both trans Pr1–Pr3 edges to form metal chains (crossed ellipsoids) with a period of b (4.281 Å) and Pr1–Pr1 side edges in two such chains related by $b/2$ to form double chains. Sufficient shared iodine remains to bridge all cluster edges and to interconnect chains at metal vertices.

Several aspects of the interchain bonding can be seen more clearly in a different view in Figure 2. Double metal chains are already known in $Sc_7Cl_{10}C_2$,[6] which contains an extra $Sc^{III}Cl_{6/2}$ cation chain that bridges between metal chains, and in $Y_6I_7C_2$,[7] $Gd_6I_7C_2$,[8] etc., where the double chains are interconnected by square planar iodine (I^{i-i}) atoms that bridge between the equivalent of Pr3–Pr3 edges. The conversion of $Y_6I_7C_2$ to the $Pr_6I_6Ru_2$ (=Pr_3I_3Ru) arrangement can be simply accomplished by shearing alternate layers of the chains in $Y_6I_7C_2$ along iodine layers (approximately parallel to $\vec{c}$) together with a translation of one layer by $b/2$. This eliminates one iodine by converting the collection of two edge-bridging iodines plus the I^{i-i} atom into two that both bridge between chains and bond to a neighboring Pr1 vertex. The coordination numbers of these I1 atoms (Figure 2) are now 5, not 4, and they exhibit a face-capping function, in contrast to the twin edge-bridging roles of I2 and I3 in the usual description of the chain in terms of metal octahedra. The shortness of the Pr3–I1 bond in this capping mode, 3.30 Å, evidently reflects the forced displacement of I1 out of a planar bridging position (∠Pr1–I1–Pr3(interchain) = 170.5°). The C-centering in $R_6I_7Z_2$ is lost in

Table IV. Important Distances (Å) and Angles (deg) in R_3I_3Z Phases

	Pr_3I_3Ru	Y_3I_3Ru	Y_3I_3Ir
		Distances[a]	
R1–R1	3.949 (1)	(4.611 (3))	(4.721 (2))
R1–R2 (×2)	3.955 (1)	3.658 (3)	3.666 (2)
R1–R3	3.807 (1)	3.500 (3)	3.518 (2)
R1–R3 (×2)	3.974 (1)	3.659 (3)	3.596 (2)
R2–R3 (×2)	3.915 (1)	3.693 (2)	3.719 (2)
Z–R1	2.864 (1)	2.870 (3)	2.904 (1)
Z–R1 (×2)	2.884 (1)	2.725 (2)	2.767 (1)
Z–R2	2.571 (1)	2.772 (3)	2.755 (1)
Z–R3 (×2)	2.851 (1)	2.776 (2)	2.773 (1)
Z–R3	(4.804 (1))	3.503 (3)	3.378 (1)
Z–Z (×2)	(4.711 (1))	3.163 (3)	3.1433 (7)
R1–I1[b] (×2)	3.493 (1)	3.301 (2)	3.280 (1)
R1–I3	3.403 (1)	3.221 (2)	3.192 (2)
R2–I2 (×2)	3.210 (1)	3.100 (2)	3.105 (1)
R2–I3 (×2)	3.268 (1)	3.197 (2)	3.197 (1)
R2–I3[b]	3.471 (1)	3.429 (2)	3.427 (2)
R3–I1	3.304 (1)	3.411 (2)	3.379 (2)
R3–I1[b] (×2)	3.416 (1)	3.409 (2)	3.450 (1)
		Angles	
R1–Z–R1 (×2)	86.79 (2)	111.20 (6)	112.72 (3)
R1–Z–R1	95.78 (2)	100.7 (1)	100.01 (5)
R1–Z–R2	179.35 (3)	155.81 (8)	153.67 (3)
R1–Z–R2 (×2)	92.77 (2)	83.43 (6)	83.21 (3)
R1–Z–R3 (×2)	88.11 (2)	79.0 (7)	78.57 (3)
R1–Z–R3	83.18 (1)	80.77 (6)	78.84 (3)
R1–Z–R3	174.87 (3)	166.84 (8)	167.78 (4)
R2–Z–R3 (×2)	92.31 (2)	83.47 (6)	84.57 (3)
R3–Z–R3	97.35 (2)	98.24 (9)	99.67 (5)
R1–I1–R3 (×2)	71.50 (1)	66.04 (5)	65.35 (3)
R1–I1–R3	170.51 (2)	172.80 (6)	171.93 (5)
R1–I1–R1	75.59 (1)	78.94 (7)	80.52 (4)
R3–I1–R3	77.61 (1)	76.00 (7)	75.80 (3)
R3–I1–R3 (×2)	99.05 (2)	107.70 (5)	108.09 (5)

[a] All atoms also have two like neighbors at ±b, 4.18–4.28 Å (Table I). [b] Interchain bridging.

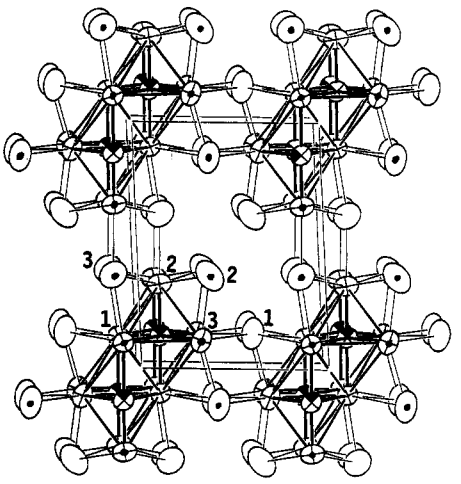

Figure 1. Section of the structure of Pr_3I_3Ru viewed slightly off the chains and [010]. The a axis is horizontal, and iodine atoms are open, praseodymium crossed, and ruthenium shaded (90% probability) ellipsoids. Pr–Ru and Pr–Pr bonds outlining the centered octahedra are emphasized. The chain contains centers of symmetry at 0, 0, 0 and 0, $^1/_2$, 0. All atoms occur at $y = {}^1/_4$ and $^3/_4$, with the latter dotted.

(16) Mattausch, Hj.; Schwarz, C.; Simon, A. *Z. Kristallogr.* **1987**, *178*, 158.
(17) Simon, A. Private communication, 1991.

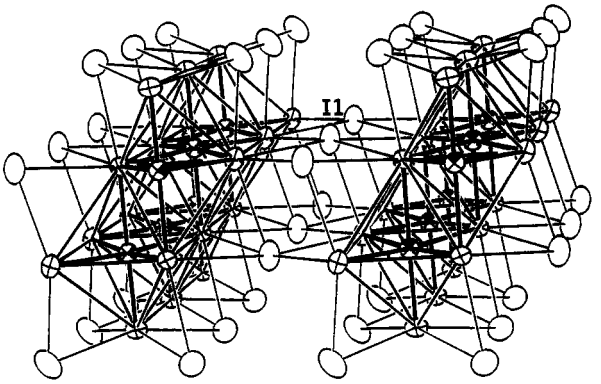

Figure 2. Portions of two chains in Pr_3I_3Ru showing the chain connectivity and interchain bridging by I1. Distinctions between atom types and positions are the same as in Figure 1 (50% ellipsoids).

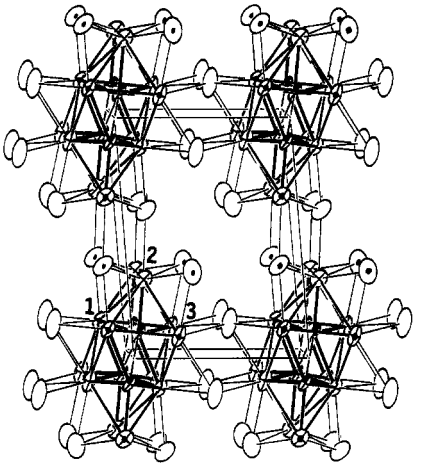

Figure 3. Section of Y_3I_3Ir viewed slightly off [010] and with $\vec{a}$ horizontal. Iodine atoms are open, yttrium crossed, and iridium shaded (75%) ellipsoids. Y–Ir and Ir–Ir bonds are emphasized, while the additional longer Y3–Ir bonds are shown as lighter lines. The symmetry is the same as in Figure 1.

the above process, and the chains in R_3I_3Z become better aligned in the second direction within [100] planes via pairs of the more usual Pr2–$I3^{a-i}$ bridges (Figure 1).

Many dimensions in the new Pr_3I_3Ru phase are, not surprisingly, close to those in the recently described Pr_4I_5Ru,[4] which consists of single chains of Ru-centered octahedra that are also interconnected by planar I^{i-i} atoms bridging side edges of octahedra in adjoining chains. The short separation between the vertex metal (Pr2) and the interstitial seen previously[4] persists with Pr_3I_3Ru, and preferred $d\pi$–$d\pi$ bonding between the interstitial and the metal vertex in the elongated Pr_6Ru octahedra again seems likely. The length of the shared edge within the chains (Pr1–Pr3) has decreased by 0.21 Å from that in Pr_4I_5Ru, while the repeat distances along the chains are very similar. The average d(Pr–Ru), 2.82 Å, is very close to that in the trigonal prismatic configuration in Pr_5Ru_2, 2.81 Å.[18]

Y_3I_3Z (Z = Ir, Ru). This structure represents the extreme of a more or less continuous distortion of the Pr_3I_3Ru structure that leads to the virtual disappearance of metal octahedra as conceptual building blocks. A clear contrast exists between the section of the Y_3I_3Ir structure shown in Figure 3 and that for Pr_3I_3Ru in Figure 1. Basically, the top five rare-earth-metal atoms that define most of one of the two chains of centered octahedra (together with their iodine sheath) are systematically displaced along $\vec{a}$ until these yttrium atoms are virtually over the lower five, while a displacement difference of $b/2$ between the "chains" is retained. (Centers of symmetry at 0, 0, 0 and 0, $^1/_2$, 0 are also kept.) In the process, the apex–Z–apex angle (R2–Z–R1) in each chain

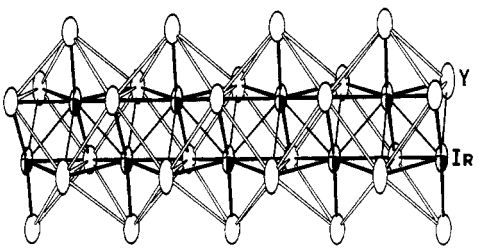

Figure 4. Side view of the Y_3Ir chain in Y_3I_3Ir with the Y–Ir bonding emphasized. The new longer Ir–Ir and Y3–Ir interactions (see text) are marked by lighter lines. Y atoms are open and Ir shaded (90%) ellipsoids.

Table V. Significant Distance Differences (Å) and Metal–Metal Bond Orders in Pr_3I_3Ru, Y_3I_3Ru, and Y_3I_3Ir

	Pr_3I_3Ru	Y_3I_3Ru	Y_3I_3Ir
av d(R–R) (no./$R_6I_6Z_2$)[a]	3.917 (9)	3.628 (8)	3.625 (8)
d_1(R)[b]	3.30	3.24	3.24
av R–R BO[a]	0.094	0.226	0.228
tot. R–R BO per $R_6I_6Z_2$[c]	0.985	1.938	1.984
av d(R–Z)[d]	2.818	2.774	2.790
addnl d(R3–Z)	(4.804)	3.503	3.378
av d(R–Z) in ref compd[d]	2.829	2.693[e]	2.704
ref compd (source)	Pr_4I_5Ru (4)	$Y_6I_{10}Ru$ (2)	$Y_6Ir_{10}Ir$ (3)
d(chain repeat): Z–Z, R–R, I–I	4.281	4.239	4.184
d_1(Z)[d]	2.50	2.50	2.53
addnl d(Z–Z)[f] (×2)	(4.18)	3.163	3.143
Z–Z BO (each)		0.08	0.10

[a] The chain repeat is omitted in these calculations. [b] The single-bond metallic distances d_1 are calculated from data in ref 19. [c] (BO for $\bar{b}$ repeat)(6) + (av R–R BO)(no.). [d] All Z have six close R neighbors. [e] This averages over a significant and poorly understood tetragonal compression within the cluster. [f] Across the double chain.

octahedron changes from 179.4 to 153.7°. The resulting metal chain, seen as a side view in Figure 4, can also be regarded as an unusual base-to-base bonding of chains of edge-sharing square prismatic Y_5Ir units such that these alternate in their top and bottom placements by half the chain repeat. The placement is not quite perfect; the long diagonals Y3–Y3 and Y1–Y1 best visualized in Figure 3 still differ by 13%, and the longer Y1–Ir and Y3–Ir distances across the middle, by 0.47 Å. New Ru–Ru contacts between interstitial atoms that were once in the separate octahedral chains also appear, as discussed below.

The third compound quantified, Y_3I_3Ru, is closely related to Y_3I_3Ir but is not quite as distorted (Table IV). The difference of standard metallic radii for Ru and Ir is ~+0.04 Å,[19] while that for the shorter Y–Z distances in the two phases is about 0.017 Å. The observed variation in $\bar{d}$(Y–Z) in the corresponding $Y_6I_{10}Z$ cluster phases is similar, +0.01 Å, but this is also accompanied by a substantial decrease in distortion within the separate octahedra when Ru is replaced by Ir.[3]

The more major changes in distances for this series and some derived bond orders are listed in Table V. A principal reason for the unusual distortion would appear to be the shorter distances and, presumably, increased bonding achieved for both R–R and Z–Z in the yttrium (and related) cases with relatively larger Z and smaller R. (Comparative bond energies for Pr–Ru vs Y–Ru would be useful in this consideration.) Lattice dimensions suggest that the same effects occur with the Er_3I_3Ru and Gd_3I_3Ir examples (Table I). The average R–R distances in the three known cases decrease 0.29 Å on formation of the yttrium examples (Table V), significant with respect to differences of only ~0.06 Å in the single-bond reference values.[19] The distortion is accompanied by the loss of one significant R–R interaction in Pr_3I_3Ru, the Pr1–Pr1 shared edge between separate chains. Even so, the bond order for the average R–R bond length with yttrium is over twice that

(18) Palenzona, A. *J. Less-Common Met.* **1979**, *66*, 27.

(19) Pearson, W. B. *The Crystal Chemistry and Physics of Metals and Alloys*; Wiley-Interscience: New York, 1972; p 151.

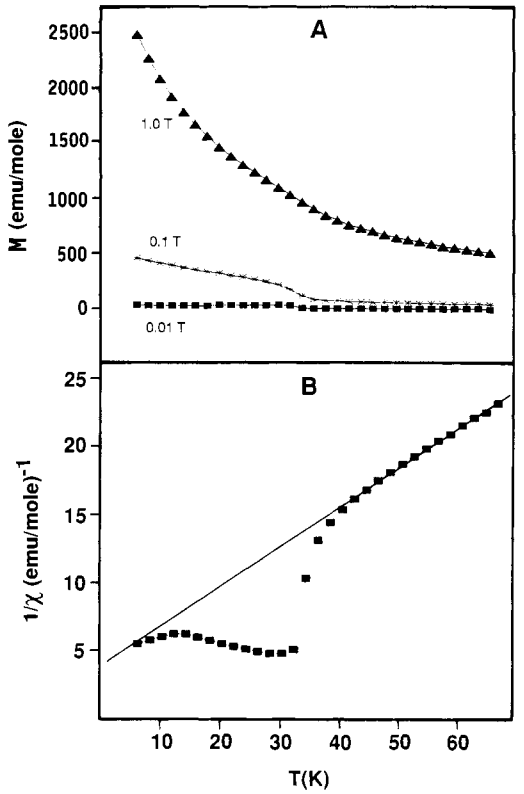

Figure 5. (A) Molar magnetization vs T for Pr_3I_3Ru at 0.01 (■), 0.1 (✱), and 1.0 T (▲). (B) $1/\chi$ (molar) for Pr_3I_3Ru as a function of T at 0.01 T. The straight line is the linear least-squares fit of the data for $50 < T < 300$ K.

with praseodymium (Table V). Since there is also a 0.10-Å decrease in the chain repeat b in the series, distances that are significant with respect to the Pr_3I_3Ru averages, we have also summed bond orders over all independent separations in the $R_6I_6Z_2$ unit. These also indicate that R–R bonding appears to roughly double on transition to these distorted structures.

The six shorter R–Z distances in the new compounds are not very different. In comparison with those in other structures like Pr_4I_5Ru and $Y_6I_{10}Z$ (Table V), the Pr–Ru examples are quite similar, while $\bar{d}$(Y–Z) values in the Y_3I_3Z examples are 0.07–0.09 Å greater. On the other hand, a seventh longer R3–Z interaction (~3.40 Å) develops between the formerly distinguishable chains with yttrium and without much elongation of the counter R1–Z separation. The apical R2–Z distance that was observed to be short in Pr_3I_3Ru (as it was in Pr_4I_5Ru) is now not particularly distinctive, as Z has moved ~0.2 Å away on distortion.

Important Z–Z interactions appear to develop during the distortion as well. Iridium is displaced 0.125 Å out of the Y1–Y3–Y1–Y3 waist plane in Y_3I_3Ir and toward two neighboring Ir interstitials. The Z–Z distance, 3.143 Å (3.163 Å in Y_3I_3Ru), corresponds to a seemingly significant bond order of 0.10 (0.08) for each of two contacts. These Z–Z interactions and the long R3–Z bond noted before are marked with narrower lines in Figure 4. Clearly, all of the changes in bonding would be better described in a delocalized band picture, but they would at the same time be more difficult to quantify in this way.

The R–I distances observed in the series follow the cluster distortions fairly well. The latter induce a wavy character in what were fairly well defined $\bar{1}02$ planes containing iodine and interstitials (compare Figures 1 and 3). The R1–I1 (bridge) and the neighboring R1–I3 distances shorten ~0.20 Å with the structure changes, while the remaining R3–I1 bridge and the capping R3–I1 bonds lengthen as R3 moves away. The remaining d(R–I) show fairly normal contractions expected on the basis of ~0.1-Å decrease in crystal radii from Pr to Y.[20]

(20) Shannon, R. D. *Acta Crystallogr.* **1976**, *A32*, 751.

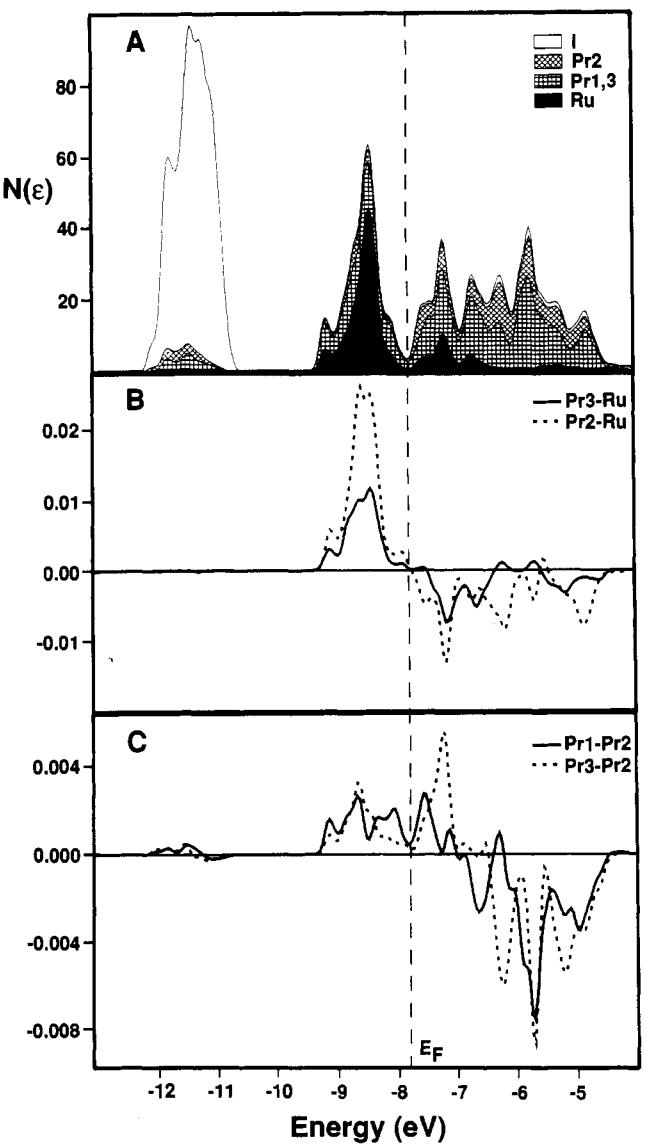

Figure 6. (A) Densities-of-states $N(\epsilon)$ vs energy calculated for Pr_3I_3Ru with atomic contributions projected out as Pr1 + Pr3 and Pr2 (apical) with hatched shading, Ru with solid, and I with open areas. The dashed line marks E_F. (B) COOP (overlap-weighted pair population) curves for Pr3–Ru (solid) and Pr2–Ru (dashed) interactions. The two types of Pr1–Ru interactions not included resemble one each of those illustrated. (C) COOP curves for Pr1–Pr2 (solid) and Pr2–Pr3 (dashed) interactions. The other Pr–Pr results have much the same character as those shown.

Properties. Magnetically, Pr_3I_3Ru shows only a normal Curie–Weiss behavior of the $4f^2$ cores in the host over the range 50–300 K. (A closed-shell behavior for the metal interstitial is normal and expected.[1]) The magnetic data yield a Weiss constant of −30 K and a slope of 3.3 μ_B per Pr, compared with 3.58 μ_B for the ideal ion. A closer value is found for Pr_4I_5Ru, 3.6 μ_B.[4] The behavior of weakly paramagnetic La_3I_3Ru is more informative regarding the band characteristics discussed below. The molar susceptibility corrected for core contributions is virtually constant, $\sim 5.4 \times 10^{-4}$ emu mol^{-1} over the range 20–150 K, rising about 20% by 300 K.

The low-temperature data for Pr_3I_3Ru in Figure 5 are unusual. The temperature dependencies at low field in parts A and B may be speculatively interpreted in terms of a ferrimagnetic transition near 32 K at low fields (0.01 T), presumably within the chains. This may be followed by some sort of weak antiferromagnetic coupling between the chains at lower temperatures, both being overwhelmed at higher fields. We have not investigated possible time-dependent or hysteresis effects.

Extended Hückel band calculations on the 1-D Pr_3I_3Ru [the sheathed $Pr_6I_6Ru_2(I^-)_4^{4-}$ actually] show the familiar pattern al-

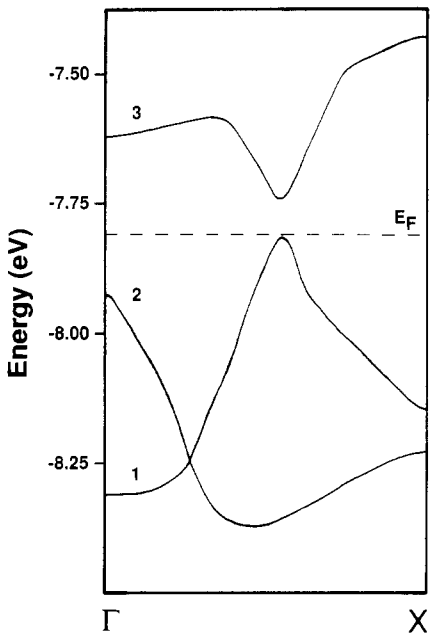

Figure 7. Behavior of the three energy bands near E_F in Pr_3I_3Ru. Bands 1 and 3 exhibit a symmetry-forbidden crossing.

ready known for Pr_4I_5Ru chains as well as for isolated, metal-centered clusters. A low-lying iodine 5p band with some admixing of host metal d orbitals reflects the binding of the iodine sheath about the cluster unit. As shown in Figure 6, the dominant Pr–Ru bonding in Pr_3I_3Ru is centered ~0.6 eV below E_F (part A), the strong Pr–Ru and Pr–Pr bonding in this region being emphasized by the COOP curves (parts B and C). Note the clear polar covalent nature of the Pr–Ru bonding and the marked segregation of the Ru population, largely 4d, into the lower region of the Pr bands, which are mainly 5d in character. Of course, the 14 electrons per Pr_3I_3Ru available for metal–metal bonding cannot all be accommodated in bonds derived solely from occupation of just the five d and one s orbitals on Ru; i.e., there must also be some Pr–Pr bonding, as suggested by the dimensional and structural details.

The calculated overlap populations for both Pr–Ru and Pr–Pr pairs vary more or less inversely with the distances. The Pr–Pr interactions remain bonding above E_F, while Pr–Ru (the apical Pr2–Ru especially) becomes sharply antibonding (Figure 6B,C), in contrast to the behavior found for Pr_4I_5Ru. This may be partly why electron-richer interstitials (Rh, Ir, Pt, etc.) have not been incorporated into the undistorted structure. The band characters near E_F (Figure 7) reflect an apparent small gap and at least a pseudo-closed-shell system that is implied by Figure 6 as well. The presence of mirror symmetry in the chains leads to the forbidden crossing of bands 1 and 3 and a small gap at E_F, ~0.1 eV, largely through a change in sign of the Pr1–Ru and Pr2-(axial)–Ru contributions in bands 1 and 3, respectively, to otherwise bonding contributions of Pr1–Pr3. Band 2 is largely axial Pr1–Ru–Pr2 bonding. The ~0.2-eV indirect gap predicted between bands 2 and 3 with no restrictions on crossing is, of course, sensitive to the choice of input parameters as well as quantitative limitations of the calculational method. Moving the Ru atoms toward each other or off the Pr1–Ru–Pr2 axis (as observed) would both lower band 3 and, in the latter case, raise band 2 and decrease the gap. These of course reflect relatively weak interactions and are the consequences, not the cause, of the beginnings of distortion found in the yttrium and other analogues. The latter involve strong bonding changes in the lower lying energy bands.

The only other predicted (and confirmed) semiconductors among the cluster chain halides are the true binaries Gd_2Cl_3, Y_2Cl_3, and their few analogues.[21-23] The small and reactive crystals available for Pr_3I_3Ru will make a direct measurement of the conductivity characteristics difficult.

Acknowledgment. Jerome Ostenson and Douglas K. Finnemore kindly provided the magnetic susceptibility data. Masahiro Ebihara prepared the Gd_3I_3Ir and Er_3I_3Ru samples. This research was supported by the National Science Foundation, Solid State Chemistry, via Grants DMR-8318616 and -8902954 and was carried out primarily in the facilities of Ames Laboratory, DOE.

Supplementary Material Available: Tables of additional diffraction and refinement data and anisotropic displacement parameters for Pr_3I_3Ru, Y_3I_3Ru, and Y_3I_3Ir (2 pages); listings of observed and calculated structure factors for the same three structural studies (20 pages). Ordering information is given on any current masthead page.

(21) Bullett, D. W. *Inorg. Chem.* **1985**, *24*, 3319.
(22) Ebbinghaus, G.; Simon, A.; Griffith, A. *Z. Naturforsch.* **1982**, *37A*, 564.
(23) Bauhofer, W.; Simon, A. *Z. Naturforsch.* **1982**, *37A*, 568.